Supplementary Material for:

Key Determinants of Selective Binding and Activation by the Monocyte Chemoattractant Proteins at the Chemokine Receptor CCR2

Zil e Huma, Julie Sanchez, Herman D. Lim, Jessica L. Bridgford, Cheng Huang, Bradyn J. Parker, Jiann G. Pazhamalil, Benjamin T. Porebski, Kevin D. G. Pfleger, J. Robert Lane, Meritxell Canals and Martin J. Stone

Detailed Materials and Methods

Materials

Dulbecco's Modified Eagle Medium (DMEM) and Hanks's balanced salt solution (HBSS) were from Invitrogen. Blasticidin and HygroGold were from InvivoGen (San Diego, CA). Foetal bovine serum was from In Vitro Technologies (Noble Park, VIC, Australia). Polyethyleneimine was from Polysciences, Inc. (Warrington, PA). Coelenterazine h was from NanoLight (Pinetop, AZ). All the other reagents were purchased from Sigma-Aldrich.

Chimeric Chemokine Constructs

Ten chimeras of human chemokines MCP-1 (obligate monomeric mutant P8A) and MCP-3 were designed based on the aligned sequences (Fig. 2). We chose to use MCP-3 rather than MCP-2 for these chimeras for the following reasons: (1) The sequence of MCP-1 is more closely related to MCP-3 (71% identity) than to MCP-2 (61% identity), allowing us to more easily draw conclusions about the roles of specific residues; (2) Both MCP-3 and the MCP-1(P8A) mutant used here are monomeric, whereas MCP-2 exists in equilibrium between monomeric and dimeric forms, potentially complicating the interpretation of chimera experiments if MCP-2 were used (especially determining whether the chimeras were correctly folded); (3) MCP-2 gives a very weak signal in the β-arrestin 2 recruitment assay so there may not have been a large enough window to reliably measure any decreases in efficacy when assessing the effects of chimeras, whereas MCP-3 gives a slightly higher signal (larger window) that allows for "confident" detection of both increases and decreases in efficacy; and (4) in our expression system, MCP-3 gives a higher yield than MCP-2 so preparation of chimeras was expected to be more straightforward. Each chimera consisted of the sequence of one chemokine with one or more of the following three regions replaced by the corresponding residues from the other chemokine: N-terminus (residues 1-10); N-loop (residues

12-24); β3 region (residues 46-52). For N-loop substitutions, residue V22 (MCP-1) or K22 (MCP-3) was not replaced and, for β3 region substitutions, residue I46 (MCP-1) or K46 (MCP-3) was not replaced because these residues are buried in the hydrophobic core and mutation would be expected to disrupt the protein fold. Genes encoding the chimeras (with an N-terminal His-tag and modified thrombin cleavage site for tag removal) were constructed by recursive PCR using overlapping oligonucleotides. The PCR products were ligated into the *NcoI/XhoI* (MCP-1 background) or *NcoI/BamHI* (MCP-3 background) restriction sites of the pET28a plasmid and transformed into DH5α *E. coli*. Colonies containing recombinant plasmids were screened by PCR and verified by DNA sequencing. Amino acid sequences of the chemokines and chimeras are listed in fig. S7.

Chemokine Expression and Purification

All chemokines and chimeras were expressed and purified as described by Tan *et al* (*1*). Briefly, the N-terminal His_6-tagged protein was expressed from BL21 (DE3) *E.coli* in LB media by induction with IPTG. Inclusion bodies containing the fusion proteins were isolated and dissolved in denaturing buffer and then purified by Ni^{2+}-affinity chromatography. The fusion protein was refolded by drop-wise dilution, the His_6-tag was removed using human thrombin and the untagged protein (containing the native N-terminus) was further purified by size exclusion chromatography. Purity was evaluated by SDS-PAGE and protein identity was confirmed by MALDI-TOF mass spectrometry (Table S3). For NMR, samples were exchanged into 20 mM sodium acetate-d_4, pH 7.0 containing 5% D_2O. ^1H NMR spectra were recorded at 25 °C, referenced to external DSS, on a Bruker Avance 600 MHz NMR spectrometer equipped with a triple-resonance cryoprobe and analysed using Bruker TopSpin software.

Homology Modelling of CCR2: chemokine complexes

To guide mutant selection, a homology model of human CCR2 bound to human MCP-1 was constructed based on the crystal structure of CXCR4 bound (and cross-linked) to the viral chemokine vMIP-II (PDB code: 4RWS) (*2*). Briefly, the sequences of CCR2 and CXCR4 were aligned by pairwise sequence alignment and the program Modeller v. 9.12 (*3*) was used to construct 3D models of CCR2 based on the CXCR4 coordinates. The best CCR2 model, selected based on Molpdf and DOPE-HR scores, was overlaid with CXCR4 and the structure of MCP-1 (single protomer extracted from PDF file 1DOM) was overlaid with vMIP-II in the 4RWS structure. The aligned structures were then used to build a composite model of CCR2 bound to MCP-1. Chain termini were capped with neutral groups (acetyl and methylamide). Residues were protonated according to their states at pH 7.

Completed structures were inserted into a palmitoyl oleoyl phosphatidyl choline (POPC) bilayer measuring 85 Å by 85 Å then solvated in a rectangular simulation box leaving at least 46 Å of water on either side of the bilayer using the CHARMM-GUI membrane builder (*4*). System charges were neutralized with respective sodium and chloride counter ions. Proteins, ions and lipids were modeled using the CHARMM36 Additive Force Field (*5, 6*) and waters were represented using the 3-particle TIP3P model (*7*). All bonds involving hydrogen atoms were constrained to their equilibrium lengths with the SHAKE algorithm (*8*). The resulting systems were subjected to at least 10,000 energy minimization steps to remove any clashes, followed by an equilibration protocol. During equilibration, we applied harmonic positional restraints of 10 $kcal^{-1}$ mol^{-1} $Å^{-2}$ to the protein backbone atoms, pressure was kept at 1 atm using the Berendsen algorithm (*9*) and the temperature was increased from 10 K to 310 K as a linear function of time over the course of 1 ns, with Langevin temperature coupling. Relaxation times for temperature and pressure were 0.5 ps. Subsequently, we removed the restraints and performed a 5 ns

simulation at constant isotropic pressure of 1 atm and temperature of 310 K. Electrostatic interactions were computed using a 10 Å cutoff radius and the Particle Mesh Ewald method for long-range interactions (*10*). All MD simulations (equilibration and production) were carried out under periodic boundary conditions.

Production simulations were carried out in the NVT ensemble. Temperature was kept at 310 K using the Langevin thermostat with a collision frequency of 2 ps. The simulation time step was 2 fs and snapshots were taken every 100 ps. Simulations were run once with Amber 14 (D.A. Case et al., University of California, San Francisco), using PMEMD on a Nvidia K20m GPU for 100 ns. The structural conformation after 100 ns was used in subsequent structural analysis.

Construction and expression of CCR2 mutants

Individual CCR2 residues or pairs of residues were selected for mutation based on their locations and orientations in the predicted chemokine binding site on the interior of the TM helical bundle. The wild type c-Myc-FLAG-CCR2 construct in pcDNA5/FRT/TO (*1*) was used as a template for Quikchange site-directed mutagenesis to generate CCR2 mutants. Wild type and mutant c-Myc-FLAG-hCCR2 constructs were transfected in HEK293 Flp-In TRex cells using Lipofectamine (Invitrogen). Cells were selected and maintained in Dulbecco's Modified Eagle Medium (DMEM) supplemented with 5% v/v tetracycline-free foetal bovine serum (FBS), 5 μg/ml blasticidin and 200 μg/ml HygroGold at 37°C in 5% CO_2 humidified incubators. Receptor expression was induced 24 h prior to each experiment by addition of 10 μg/ml tetracycline.

Cell surface expression: Whole cell ELISA.

The cell surface expression of CCR2 was measured using anti-c-Myc ELISA as previously described (*11*). Primary antibody anti-c-Myc (9E10) was diluted 1:2000 in TBS/0.1% w/v BSA. Secondary antibody, anti-mouse-HRP was diluted 1:2000 in blocking buffer. Data were normalized as the

ratio of OD_{490} of mutants over the OD_{490} of the wild type CCR2. For internalization experiments, cells were stimulated with 100 nM of chemokine in full media and incubated for one hour at 37 °C, and rinsed with DMEM at pH 2.5 prior to fixation (*11*). All experiments were repeated at least three times and performed in triplicate.

Membrane preparation and radioligand binding assays

Cell membranes were prepared by detaching the cells from the flasks, centrifugation at 1500g for 3 min and resuspension in ice-cold 50mM MOPS buffer with 5mM $MgCl_2$ and 0.1% 3-[(3-cholamidopropyl)-dimethylammonio]-1-propanesulfonic acid (CHAPS), pH 7.4. The lysates were homogenized by sonication and centrifuged at low speed for 5 min. Membrane and cytosolic fractions were separated by centrifugation of the supernatants at an rcf of 40,000g for 30 min. The membrane pellet was resuspended in MOPS buffer with 5 mM $MgCl_2$ and 0.1% CHAPS, pH 7.4 and stored at -20 °C. Protein concentrations were measured using a BCA protein determination assay (*12*).

Competitive binding assays were performed as described by Zweemer *et al*. (*13*). Briefly, binding assays were performed in a 100-µl reaction volume containing 50 mM MOPS buffer (pH 7.4), 5 mM $MgCl_2$, 0.1% CHAPS, 5-20 µg of membranes, increasing concentrations of chemokines and 45 pM ^{125}I-MCP-1. Membranes were incubated for 120 min at 37°C. Nonspecific binding was determined in the presence of 10 µM INCB3344. Binding was terminated by dilution with ice-cold 50 mM MOPS buffer supplemented with 0.05% CHAPS and 0.5 M NaCl followed by rapid filtration through a 96-well GF/C filter plate precoated with 0.5% polyethyleneimine using a PerkinElmer Filtermate-harvester (PerkinElmer, Groningen, The Netherlands). Filters were washed 3 times with ice-cold wash buffer, dried at 50°C, and 25 µl of MicroScint-O scintillation cocktail (PerkinElmer) was added to each well. Radioactivity was determined by using a MicroBeta^2 LumiJET 2460 Microplate Counter (PerkinElmer).

β-Arrestin recruitment assays

Recruitment of β-arrestin-2 to CCR2 was assessed in HEK293 Flp-In TRex transiently transfected with CCR2-RLuc8 and β-arrestin-2-YFP as previously described (*14*). Briefly, CCR2-RLuc8 and β-arrestin-2-YFP were transfected at a receptor:arrestin ratio of 1:4 using PEI at a 1:6 ratio (Scholten et al., 2012 BJP). After 24 h, cells were re-plated in poly-D-Lysine-coated 96-well white opaque CulturPlates (PerkinElmer). 48h after transfection cells were rinsed and pre-incubated in Hank's Balanced Saline Solution (HBSS) for 30 min at 37°C. Coelenterazine h was added to each well (final concentration 5 µM) followed by the immediate addition of receptor ligands. Cells were incubated for further 10 min in the dark at 37°C. BRET measurements were obtained using a PHERAstar plate reader (BMG Labtech, Ortenberg, Germany) that allows for sequential integration of the signals detected at 475 ± 30 and 535 ± 30 nm, using filters with the appropriate band pass. Data are presented as a ligand-induced BRET ratio (normalized by subtracting the BRET ratio of vehicle treated cells). All experiments were performed in triplicate and repeated independently at least 3 times.

ERK1/2 phosphorylation

Phosphorylation of ERK1/2 was measured using the AlphaScreen® SureFire® p-ERK 1/2 (Thr202/Tyr204) Assay Kit (PerkinElmer, TGR biosciences) following the manufacturer's instructions. Briefly, 4 x10^5 cells/well were seeded in a poly-D-Lysine-coated plate in full media containing 10 µg/ml tetracycline and serum starved overnight. Initial time-course experiments determined that peak levels of ERK 1/2 phosphorylation were achieved 3 min after the addition of chemokines. Therefore, for all subsequent concentration-response experiments, cells were stimulated for 3 min at 37°C. 10% v/v FBS was used as a positive control. The reaction was terminated by removal of the media and addition with 100µl of *SureFire* lysis buffer. Cell lysis was assisted by leaving the plates on a shaker at 600rpm for 5 min. 5 µl of lysate was transferred to a

white 384-well Proxiplate™ followed by the addition of 8 µl of *SureFire* AlphaScreen Detection Mix (240:1440:7:7 v/v dilution of *SureFire* Activation Buffer: *SureFire* Reaction Buffer: AlphaScreen Acceptor Beads: AlphaScreen Donor Beads). The plate was incubated in the dark for 1.5 h at 37°C and the AlphaScreen signal was read on an *Envision®* plate reader (PerkinElmer). Data were normalized between the signal in the absence of chemokine (0% response) and in the presence of 10% v/v FBS (100% response). All experiments were performed in triplicate and repeated independently at least 3 times.

Inhibition of forskolin-induced cAMP

The ability of ligands to inhibit forskolin-induced cAMP production was assessed in c-Myc-FLAG-CCR2 HEK293 FlpIn TRex cells transiently transfected to express the CAMYEL cAMP BRET biosensor (*11*). Cells were grown overnight in white poly-D-Lysine-coated 96-well Culturplates (Perkin Elmer). Transient transfection was performed using PEI at a 6:1 ratio of DNA. 48h after transfection cells were rinsed and pre-incubated in Hank's Balanced Saline Solution (HBSS) for 30 min at 37°C. Cells were then incubated with the RLuc substrate coelenterazine h, final concentration 5µM, for 5 min, followed by a further 5 min incubation with increasing concentrations of chemokine. Forskolin was then added to a final concentration of 10µM. After 5 min the YFP and the RLuc emissions were measured using a LumiSTAR Omega (BMG Labtech, Ortenberg, Germany) that allows for sequential integration of the signals detected at 475 ± 30 and 535 ± 30 nm, using filters with the appropriate band pass. BRET ratio was calculated as the ratio of YFP to RLuc signals, and data are expressed as the percentage of the forskolin-induced signal.

Data analysis and Statistics

All data points represent the mean and error bars represent the standard error of the mean (SEM) of at least three independent experiments. The results were analyzed using Prism 6.0 (GraphPad

Software Inc., San Diego, CA). All data from concentration-response curves were normalized as outlined above and fitted using the following three parameter equation (equation 1).

$$Y = bottom + \frac{top - bottom}{1 + 10^{(\log EC_{50} - \log[A])}} \qquad \text{(equation 1)}$$

where *top* and *bottom* represent the maximal and minimal asymptote of the concentration–response curve, [*A*] is the molar concentration of agonist and EC_{50} is the molar concentration of agonist required to give a response half way between bottom and top.

Concentration–response data were also fitted to the following form of the operational model of agonism (*15*) to allow the quantification of biased agonism

$$Y = basal + \frac{(E_m - basal)\left(\frac{\tau}{K_A}\right)^n [A]^n}{[A]^n\left(\frac{\tau}{K_A}\right)^n + \left(1 + \frac{[A]}{K_A}\right)^n} \qquad \text{(equation 2)}$$

where E_m is the maximal possible response of the system, Basal is the basal level of response, K_A represents the equilibrium dissociation constant of the agonist (A) and τ is an index of the signaling efficacy of the agonist that is defined as R_T/K_E, where R_T is the total number of receptors and K_E is the coupling efficiency of each agonist-occupied receptor, and *n* is the slope of the transducer function that links occupancy to response. The analysis assumes that the transduction machinery used for a given cellular pathway are the same for all agonists, such that the E_m and transducer slope (*n*) are shared between agonists. Data for all chemokines for each pathway were fit globally, to determine values of K_A and τ. Biased agonism was quantified as previously described (*16*). In short, to exclude the impact of cell-dependent and assay-dependent effects on the observed agonism at each pathway, the $\log(\tau/K_A)$ value of a reference agonist, in this case MCP-1 WT, is subtracted from the $\log(\tau/K_A)$ value of the other chemokines to yield $\Delta\log(\tau/K_A)$. The relative bias can then be calculated for each chemokine at the two different signaling pathways by

subtracting the Δlog(τ/K_A) of one pathway from the other to give a ΔΔlog(τ/K_A) value, which is a measure of bias. A lack of biased agonism will result in values of ΔΔlog(τ/K_A) not significantly different from 0 between pathways. To account for the propagation of error associated with the determination of composite parameters, the following equation was used:

$$Pooled\_SEM = \sqrt{(SEj1)^2 + (SEj2)^2} \qquad \text{(equation 3)}$$

For radioligand binding, the concentration of agonist that inhibited half of the ^{125}I-MCP-1 binding (IC_{50}) was determined using the following equation:

$$Y = \frac{Bottom + (Top - Bottom)}{1 + 10^{(X - logIC_{50})n_H}} \qquad \text{(equation 4)}$$

where Y denotes the percentage-specific binding, Top and Bottom denote the maximal and minimal asymptotes, respectively, IC_{50} denotes the X-value when the response is midway between Bottom and Top, and n_H denotes the Hill slope factor. For ^{125}I-MCP-1 homologous competition-binding experiments, estimates of affinity (K_d) were obtained using the equation:

$$IC_{50} = [Hot] + K_d \qquad \text{(equation 5)}$$

For all other chemokines IC_{50} values obtained from the inhibition curves were converted to K_i values using the Cheng and Prusoff equation (*17*).

All affinity (pK_i), potency (pEC_{50}) and transduction ratio (log(τ/K_A)) parameters were estimated as logarithms. As we have previously demonstrated that the logarithm of the measure is approximately Gaussian (*18*), and as the application of t-tests and analyses of variance assume Gaussian distribution, estimating the parameters as logarithms allows valid statistical comparison. Multiple T test comparison with Holm-Sidak correction or one way ANOVA were used as stated in Figure Legends. Significance is defined as * for $p < 0.05$, ** for $p<0.01$ and *** for $p < 0.001$ for the comparison graphs.

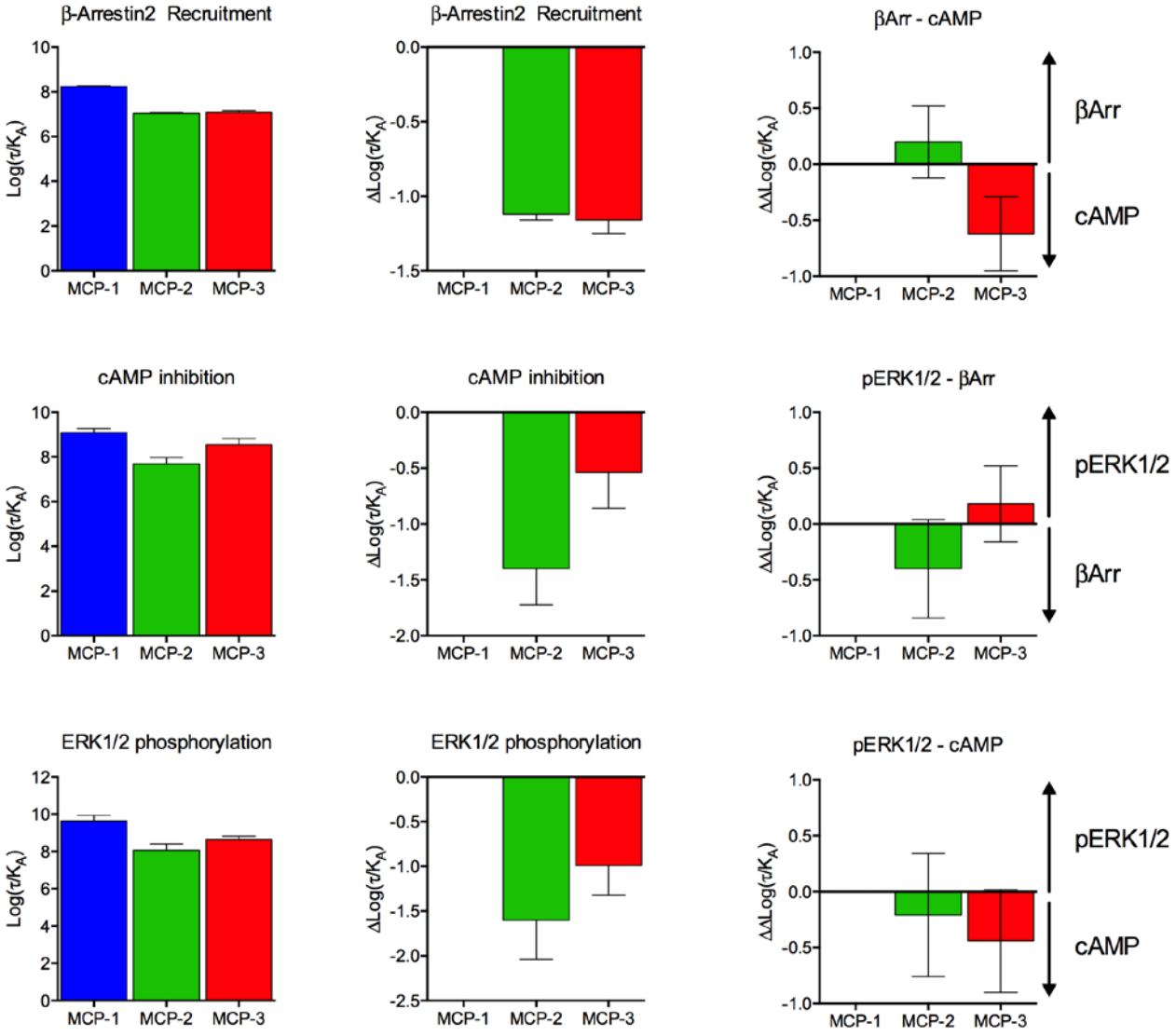

Figure S1. Neither MCP-2 nor MCP-3 are biased agonists at CCR2 relative to MCP-1. Fitted (left) and normalized (center) transducer ratios for MCP-1 (blue), MCP-2 (green) and MCP-3 (red) in β-arrestin 2 recruitment BRET, inhibition of forskolin-induced cAMP and ERK1/2 phosphorylation pathways. Bias factors between pathways ($\Delta\Delta\text{Log}(\tau/K_A)$) (right), calculated from the data shown in Figure 1, indicate the absence of biased agonism.

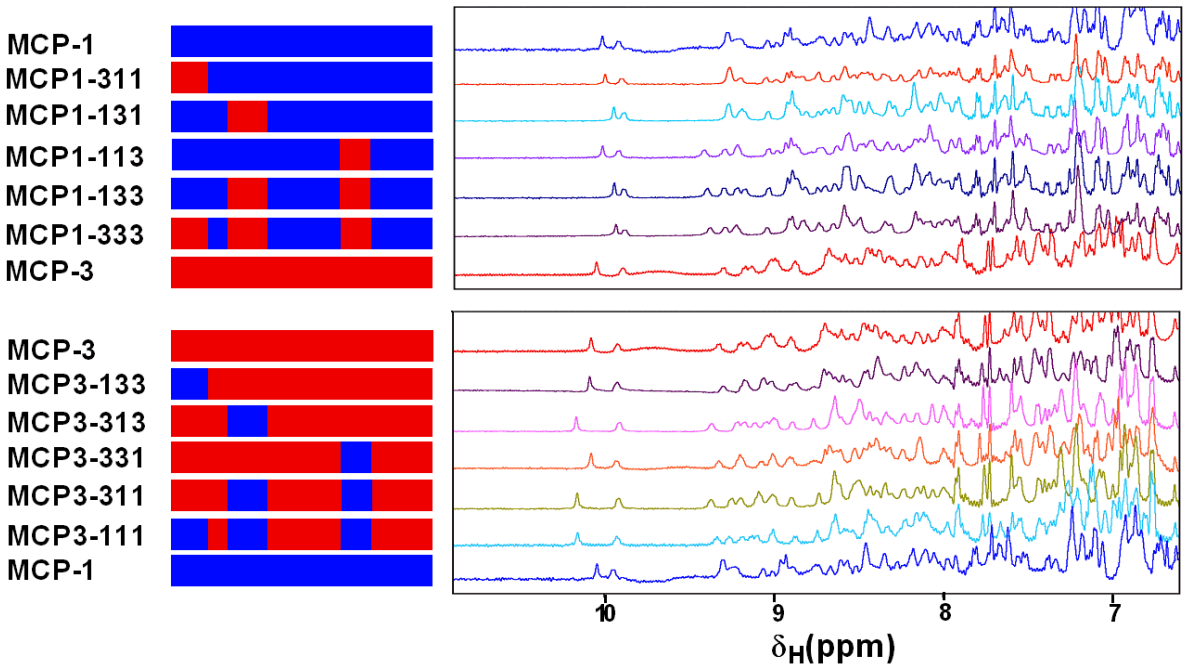

Figure S2. Downfield (amide and aromatic) region of the ^{1}H NMR spectra of WT and chimeric chemokines, showing well-dispersed peaks indicative of correct folding. The names and schematic diagrams of the chimeras are shown on the left with regions from MCP-1 and MCP-3 in blue and red, respectively.

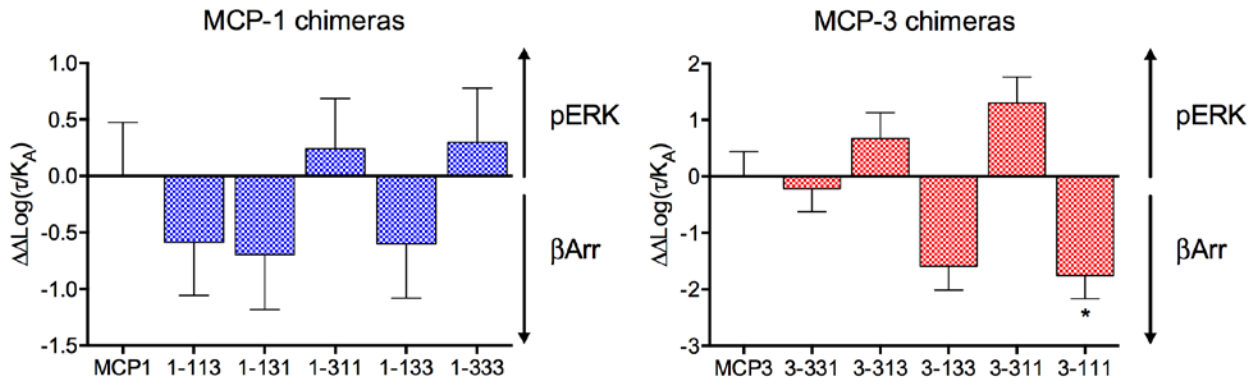

Figure S3. MCP3-111 displays biased agonism relative to MCP-3. Bias factors ($\Delta\Delta\text{Log}(\tau/K_A)$) between β-arrestin 2 recruitment and ERK1/2 phosphorylation, calculated from the data shown in Figure 3, show that the chimeric chemokine MCP3-111 is significantly (P <0.05) biased towards β-arrestin 2 recruitment compared to MCP-3.

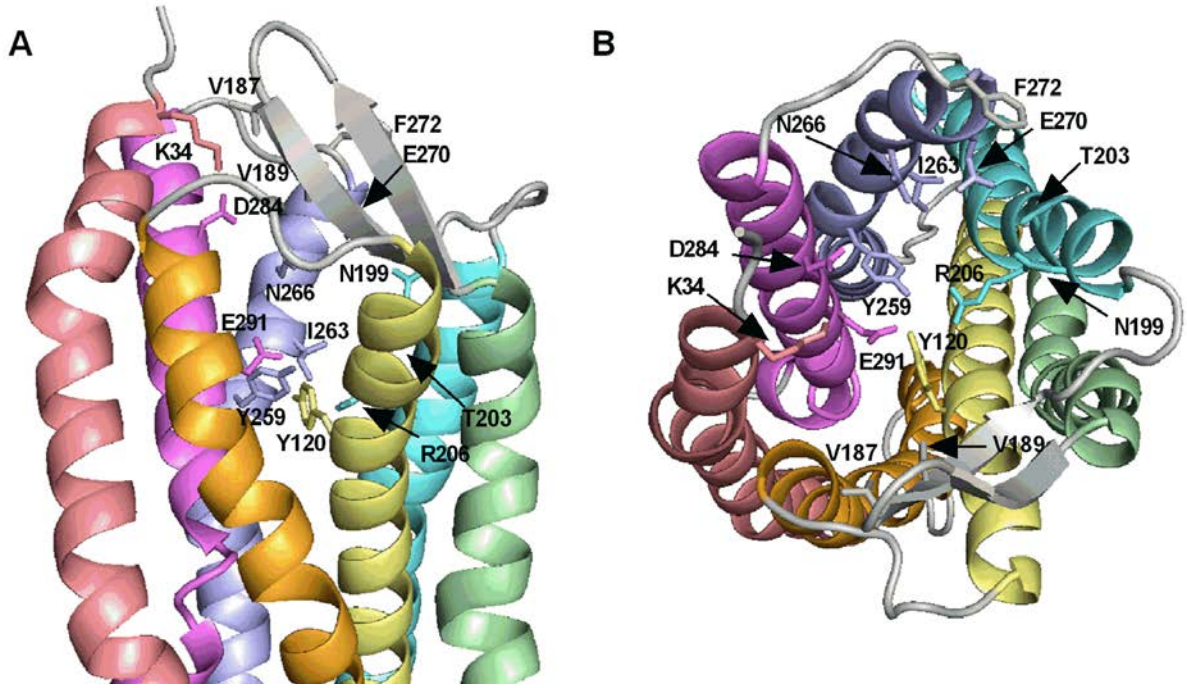

Figure S4. Homology model of CCR2 bound to MCP-1, showing the positions of the mutated residues. (A) Side view and **(B)** end-on view (from the extracellular perspective). CCR2 transmembrane helices are coloured salmon (TM1), orange (TM2), pale yellow (TM3), pale green (TM4), aquamarine (TM5), light blue (TM6) and violet (TM7); other receptor residues are in grey. Side chain sticks are shown for mutated residues in the same colours as the helices/loops in which they are located.

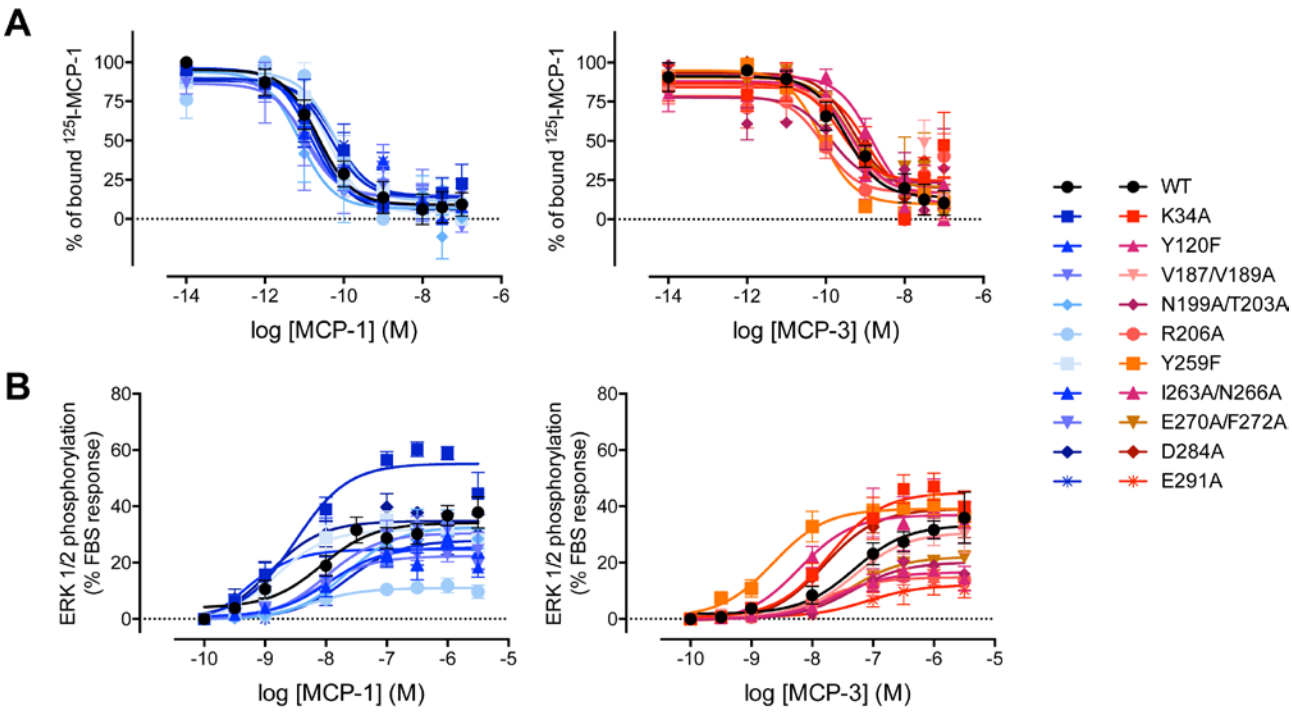

Figure S5. ^{125}I-MCP-1 competition binding and ERK1/2 phosphorylation concentration response curves for CCR2 mutants. ^{125}I-MCP-1 competition binding and ERK1/2 phosphorylation were assessed for MCP-1 and MCP-3 at the wild type (WT) and mutant CCR2 expressed in FlpInTRex 293 cells. **(A)** Competition binding curves of MCP-1 (blue) and MCP-3 (red) for WT or mutant CCR2 measured in cell membrane preparations. **(B)** ERK1/2 phosphorylation concentration response curves of MCP-1 (blue) and MCP-3 (red) for WT or mutant CCR2. Data are the mean ± SEM from 3-5 experiments performed in triplicate.

Figure S6

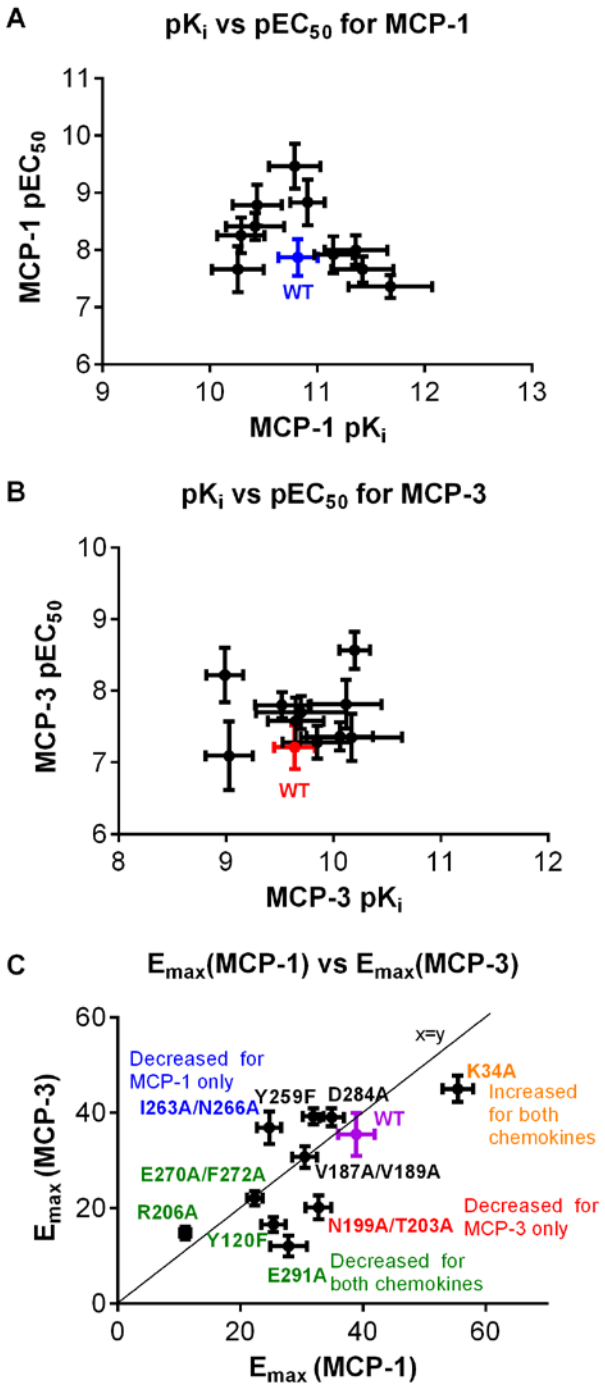

Figure S6. Graphical comparisons of chemokine binding and ERK1/2 phosphorylation parameters across the set of CCR2 mutants. (A, B) Binding affinity (pK_i) versus potency (pEC_{50}) for **(A)** MCP-1 and **(B)** MCP-3. **(C)** Efficacy (E_{max}) for activation by MCP-1 versus MCP-3.

Figure S7

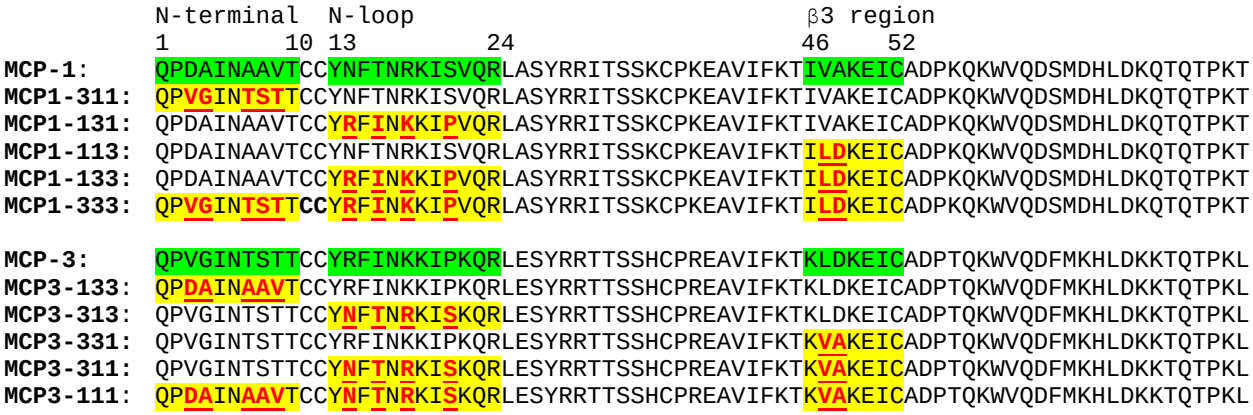

Figure S7. The amino acid sequences of MCP-1(P8A), wild type MCP-3 and the chimeric chemokines. The green highlighted regions correspond to the N terminus (1-10), N loop (12 -24) and β3 region (46-52) of MCP-1 and MCP-3, respectively. The yellow highlighted regions correspond to the regions that are mutated (from MCP-1 to MCP-3 in the five chimeras on MCP-1 background and from MCP-3 to MCP-1 in the five chimeras on MCP-3 background) and the red, bold, underlined residues are the specific mutations made.

	β-arrestin recruitment		cAMP inhibition		ERK1/2 phosphorylation		pERK - cAMP	pERK - βArr	βArr - cAMP
	log(τ/K_A)	Δlog(τ/K_A)	log(τ/K_A)	Δlog(τ/K_A)	log(τ/K_A)	Δlog(τ/K_A)	ΔΔlog(τ/K_A)	ΔΔlog(τ/K_A)	ΔΔlog(τ/K_A)
MCP-1	8.24 ± 0.03	0	9.09 ± 0.17	0	9.65 ± 0.29	0	0	0	0
MCP-2	7.04 ± 0.02	-1.12 ± 0.04	7.69 ± 0.28	-1.40 ± 0.32	8.05 ± 0.34	-1.60 ± 0.44	-0.21 ± 0.55	-0.40 ± 0.44	0.20 ± 0.32
MCP-3	7.08 ± 0.09	-1.16 ± 0.09	8.55 ± 0.27	-0.54 ± 0.32	8.66 ± 0.16	-0.99 ± 0.33	-0.44 ± 0.46	0.18 ±0.34	-0.62 ±0.33

Table S1. Biased agonism at CCR2. Fitted (Log(τ/K_A)) and normalized (ΔLog(τ/K_A)) transducer ratios for MCP-1, MCP-2 and MCP-3 in β-arrestin 2 recruitment BRET, inhibition of forskolin-induced cAMP and ERK1/2 phosphorylation pathways. Bias factors between pathways (ΔΔLog(τ/K_A)), calculated from the data shown in Figure 1, indicate the absence of biased agonism.

	β-arrestin recruitment		ERK1/2 phosphorylation		pERK - βArr
	$\log(\tau/K_A)$	$\Delta\log(\tau/K_A)$	$\log(\tau/K_A)$	$\Delta\log(\tau/K_A)$	$\Delta\Delta\log(\tau/K_A)$
MCP-1	7.41 ± 0.16	0 ± 0.23	7.74 ± 0.29	0 ± 0.41	0 ± 0.47
MCP1-311	6.23 ± 0.17	-1.17 ± 0.24	6.80 ± 0.24	-0.93 ± 0.38	0.24 ± 0.44
MCP1-131	8.02 ± 0.17	0.61 ± 0.23	7.65 ± 0.31	-0.09 ± 0.42	-0.70 ± 0.48
MCP1-113	7.76 ± 0.17	0.35 ± 0.23	7.50 ± 0.29	-0.24 ±0.41	-0.59 ± 0.47
MCP1-133	7.69 ± 0.29	0.56 ± 0.24	7.97 ± 0.18	-0.04 ± 0.41	-0.60 ± 0.48
MCP1-333	5.39 ± 0.25	-2.02 ± 0.30	6.01 ± 0.23	-1.72 ± 0.37	0.30 ±0.48
MCP-3	6.22 ± 0.17	0 ± 0.17	7.33 ± 0.26	0 ± 0.37	0 ± 0.44
MCP3-133	8.23 ± 0.17	2.01 ± 0.17	7.75 ± 0.24	0.42 ±0.35	-1.60 ± 0.42
MCP3-313	5.69 ± 0.20	-0.53 ± 0.19	7.47 ± 0.27	0.14 ±0.38	0.67 ± 0.46
MCP3-331	6.01 ± 0.18	-0.21 ± 0.18	6.90 ± 0.19	-0.43 ±0.32	-0.22 ± 0.40
MCP3-311	5.74 ± 0.21	-0.48 ± 0.21	8.14 ± 0.27	0.82 ±0.37	1.30 ± 0.46
MCP3-111	7.65 ± 0.18	1.43 ± 0.18	6.99 ± 0.20	-0.33 ±0.33	-1.76 ± 0.41 *

Table S2. MCP3-111 displays biased agonism at CCR2 compared to MCP-3. Fitted ($\mathrm{Log}(\tau/K_A)$) and normalized ($\Delta\mathrm{Log}(\tau/K_A)$) transducer ratios for MCP-1 and MCP-3 chimeras in β-arrestin 2 recruitment BRET and ERK1/2 phosphorylation pathways. Bias factors between pathways ($\Delta\Delta\mathrm{Log}(\tau/K_A)$), calculated from the data shown in Figure 3, show that only MCP3-111 displays significant bias towards β-arrestin 2 recruitment compared to its parental chemokine. * $P<0.05$ one-way ANOVA with Dunnett's multiple comparison test.

Chemokine	Expected Mass (Da)	Observed Mass (Da)
MCP-1 (P8A)	8659.0	8658.4
MCP1-311	8677.0	8675.3
MCP1-131	8695.2	8695.1
MCP1-113	8717.0	8716.8
MCP1-133	8753.2	8750.1
MCP1-333	8771.2	8768.7
MCP-3 (WT)	8956.4	8951.7
MCP3-133	8938.4	8935.1
MCP3-313	8920.3	8919.3
MCP3-331	8898.4	8892.5
MCP3-311	8862.2	8859.1
MCP3-111	8844.2	8843.2

Table S3. Expected and observed molecular masses of wild type and chimeric chemokines. Observed masses were obtained by MALDI-TOF mass spectrometry.

References

1. J. H. Y. Tan, M. Canals, J. P. Ludeman, J. Wedderburn, C. Boston, S. J. Butler, A. M. Carrick, T. R. Parody, D. Taleski, A. Christopoulos, R. J. Payne, M. J. Stone, Design and Receptor Interactions of Obligate Dimeric Mutant of Chemokine Monocyte Chemoattractant Protein-1 (MCP-1). *Journal of Biological Chemistry* **287**, 14692-14702 (2012).
2. L. Qin, I. Kufareva, L. G. Holden, C. Wang, Y. Zheng, C. Zhao, G. Fenalti, H. Wu, G. W. Han, V. Cherezov, R. Abagyan, R. C. Stevens, T. M. Handel, Structural biology. Crystal structure of the chemokine receptor CXCR4 in complex with a viral chemokine. *Science* **347**, 1117-1122 (2015).
3. N. Eswar, B. Webb, M. A. Marti-Renom, M. S. Madhusudhan, D. Eramian, M. Y. Shen, U. Pieper, A. Sali, Comparative protein structure modeling using MODELLER. *Current protocols in protein science / editorial board, John E. Coligan ... [et al* **Chapter 2**, Unit 2 9 (2007).
4. S. Jo, J. B. Lim, J. B. Klauda, W. Im, CHARMM-GUI Membrane Builder for mixed bilayers and its application to yeast membranes. *Biophysical journal* **97**, 50-58 (2009).
5. J. Huang, A. D. MacKerell, Jr., CHARMM36 all-atom additive protein force field: validation based on comparison to NMR data. *J Comput Chem* **34**, 2135-2145 (2013).
6. J. B. Klauda, R. M. Venable, J. A. Freites, J. W. O'Connor, D. J. Tobias, C. Mondragon-Ramirez, I. Vorobyov, A. D. MacKerell, Jr., R. W. Pastor, Update of the CHARMM all-atom additive force field for lipids: validation on six lipid types. *J Phys Chem B* **114**, 7830-7843 (2010).
7. W. L. Jorgensen, J. Chandrasekhar, J. D. Madura, R. W. Impey, M. L. Klein, Comparison of Simple Potential Functions for Simulating Liquid Water. *Journal of Chemical Physics* **79**, 926-935 (1983).
8. R. A. Lippert, K. J. Bowers, R. O. Dror, M. P. Eastwood, B. A. Gregersen, J. L. Klepeis, I. Kolossvary, D. E. Shaw, A common, avoidable source of error in molecular dynamics integrators. *Journal of Chemical Physics* **126**, (2007).
9. H. J. C. Berendsen, J. P. M. Postma, W. F. Vangunsteren, A. Dinola, J. R. Haak, Molecular-Dynamics with Coupling to an External Bath. *Journal of Chemical Physics* **81**, 3684-3690 (1984).
10. T. Darden, D. York, L. Pedersen, Particle Mesh Ewald - an N.Log(N) Method for Ewald Sums in Large Systems. *Journal of Chemical Physics* **98**, 10089-10092 (1993).
11. D. J. Scholten, M. Canals, M. Wijtmans, S. de Munnik, P. Nguyen, D. Verzijl, I. J. de Esch, H. F. Vischer, M. J. Smit, R. Leurs, Pharmacological characterization of a small-molecule agonist for the chemokine receptor CXCR3. *Br J Pharmacol* **166**, 898-911 (2012).
12. P. K. Smith, R. I. Krohn, G. T. Hermanson, A. K. Mallia, F. H. Gartner, M. D. Provenzano, E. K. Fujimoto, N. M. Goeke, B. J. Olson, D. C. Klenk, Measurement of Protein Using Bicinchoninic Acid. *Anal. Biochem.* **150**, 76-85 (1985).
13. A. J. Zweemer, I. Nederpelt, H. Vrieling, S. Hafith, M. L. Doornbos, H. de Vries, J. Abt, R. Gross, D. Stamos, J. Saunders, M. J. Smit, A. P. Ijzerman, L. H. Heitman, Multiple binding sites for small-molecule antagonists at the CC chemokine receptor 2. *Mol Pharmacol* **84**, 551-561 (2013).
14. M. A. Ayoub, Y. Zhang, R. S. Kelly, H. B. See, E. K. M. Johnstone, E. A. McCall, J. H. Williams, D. J. Kelly, K. D. G. Pfleger, Functional Interaction between Angiotensin II Receptor Type 1 and Chemokine (C-C Motif) Receptor 2 with Implications for Chronic Kidney Disease. *Plos One* **10**, (2015).
15. J. W. Black, P. Leff, N. P. Shankley, J. Wood, An operational model of pharmacological agonism: the effect of E/[A] curve shape on agonist dissociation constant estimation. *Br J Pharmacol* **84**, 561-571 (1985).

16. T. Kenakin, C. Watson, V. Muniz-Medina, A. Christopoulos, S. Novick, A simple method for quantifying functional selectivity and agonist bias. *ACS chemical neuroscience* **3**, 193-203 (2012).
17. Y. Cheng, W. H. Prusoff, Relationship between Inhibition Constant (K1) and Concentration of Inhibitor Which Causes 50 Per Cent Inhibition (I50) of an Enzymatic-Reaction. *Biochemical Pharmacology* **22**, 3099-3108 (1973).
18. A. Christopoulos, Assessing the distribution of parameters in models of ligand-receptor interaction: to log or not to log. *Trends Pharmacol Sci* **19**, 351-357 (1998).